Controlling the Activation at Ni^{II}—CO$_2^{2-}$ Moieties through Lewis Acid Interactions in the Second Coordination Sphere

Siad Wolff,[a] Vladimir Pelmenschikov,[b] Robert Müller,[c] Mervan Ertegi,[a] Beatrice Cula,[a] Martin Kaupp,*[b] and Christian Limberg*[a]

Nickel complexes with a two-electron reduced CO$_2$ ligand (CO$_2^{2-}$, "carbonite") are investigated with regard to the influence alkali metal (AM) ions have as Lewis acids on the activation of the CO$_2$ entity. For this purpose complexes with Ni^{II}(CO$_2$)AM (AM=Li, Na, K) moieties were accessed via deprotonation of nickel-formate compounds with (AM)N(^{i}Pr)$_2$. It was found that not only the nature of the AM ions in vicinity to CO$_2$ affect the activation, but also the number and the ligation of a given AM. To this end the effects of added (AM)N(R)$_2$, THF, open and closed polyethers as well as cryptands were systematically studied. In 14 cases the products were characterized by X-ray diffraction and correlations with the situation in solution were made. The more the AM ions get detached from the carbonite ligand, the lower is the degree of aggregation. At the same time the extent of CO$_2$ activation is decreased as indicated by the structural and spectroscopic analysis and reactivity studies. Accompanying DFT studies showed that the coordinating AM Lewis acidic fragment withdraws only a small amount of charge from the carbonite moiety, but it also affects the internal charge equilibration between the L^{tBu}Ni and carbonite moieties.

Introduction

Utilizing ubiquitous CO$_2$ as an inexpensive C$_1$-source to produce valuable chemicals and fuels is a central aim of current research efforts.[1–6] Reductive transformations typically require an initial energy input in form of heat, irradiation or electrons, which may originate from metal centres.[7–14]

In this regard, the [Ni,Fe] carbon monoxide dehydrogenase (CODH) serves as a natural role model for a reductive activation process, as it catalyses the reversible transformation of CO$_2$ to CO.[15–16] Dobbek and co-workers have succeeded in isolating an intermediate of the enzymatic cycle which features a doubly reduced CO$_2^{2-}$ "carbonite" ligand,[17] bound by a heterobimetallic [Ni,Fe] site (Figure 1).[18–19] Activation of the CO$_2$ molecule
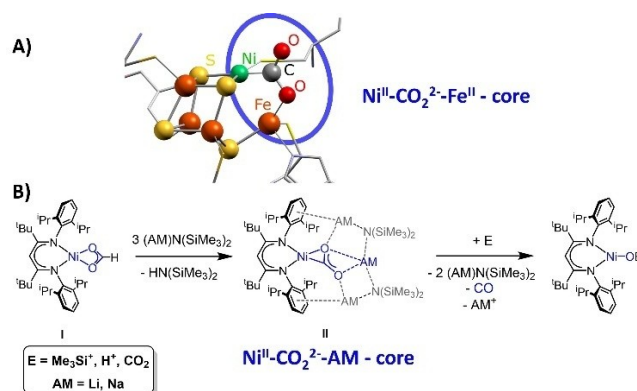

Figure 1. (A) Structure of the carbonite intermediate in the catalytic cycle of the [Ni,Fe]—CODH (A). (B) A similar species can be formed via formate deprotonation at a β-diketiminato nickel site.

[a] S. Wolff, M. Ertegi, Dr. B. Cula, Prof. Dr. C. Limberg
Institut für Chemie
Humboldt-Universität zu Berlin
Brook-Taylor-Straße 2, 12489 Berlin (Germany)
E-mail: christian.limberg@chemie.hu-berlin.de

[b] Dr. V. Pelmenschikov, Prof. Dr. M. Kaupp
Institut für Chemie
Theoretische Chemie/Quantenchemie, Sekr.C7
Technische Universität Berlin
Straße des 17. Juni 135, 10623 Berlin (Germany)
E-mail: martin.kaupp@tu-berlin.de

[c] Dr. R. Müller
Institut für Chemie und Biochemie
Physikalische und Theoretische Chemie
Freie Universität Berlin
Arnimallee 22, 14195 Berlin (Germany)

accordingly proceeds in a cooperative fashion, involving the fixation at the redox-active Ni centre as well as support by an additional Lewis acidic interaction with the Fe^{II} centre to facilitate the redox process. Chemists have shown that synthetic analogues of such metal-bound CO$_2$ complexes can be produced through reactions of gaseous CO$_2$ with reduced metal precursors under laboratory conditions[20–23] and a few representatives with nickel as the central atom have been reported.[24–27] Isolation and characterisation of corresponding low molecular weight M—CO$_2$ complexes is of high interest, since they offer the opportunity for directed investigation of the relation between structure and reactivity. Especially, the role of supporting Lewis acids in the second coordination sphere needs to be elucidated more closely, since several publications reported that their presence facilitate CO$_2$ activation processes as well as catalytic turnovers.[23,28–34] However, isolation of M—CO$_2$ species, derived from gaseous CO$_2$, can be challenging

Chem. Eur. J. **2024**, *30*, e202303112 (1 of 14)

© 2024 The Authors. Chemistry - A European Journal published by Wiley-VCH GmbH

Chemistry–A European Journal

Research Article
doi.org/10.1002/chem.202303112

Chemistry
Europe
European Chemical
Societies Publishing

due to successive reactions with excessive CO_2 leading to reductive disproportions of the desired intermediates.[35–40]

Recently, we have reported that deprotonation of the formate complex [L^{tBu}NiOOCH], **I**, with amide bases gives rise to reduced CO_2 complexes of the type [L^{tBu}Ni(CO_2)AM$_3$$(NR_2)_2$] (AM=Li, Na, K; R=N(SiMe$_3$)$_2$), **II** (Figure 1).[41] These complexes contain a Ni^{II}–CO_2^{2-} core surrounded by Lewis acidic alkali metal (AM) cations and therefore resemble the bifunctional active site of the CODH; similar structural motifs have also been found in the product resulting from CO_2 activation at a β-diketiminato Ni^0 entity.[42] For the deprotonation of the formate ligand with (AM)N(SiMe$_3$)$_2$, a threefold excess of base was required to ensure a complete conversion of **I**. While the first equivalent was needed for β-deprotonation of the formate ligand, the additional two equivalents remained in the second coordination sphere around the Ni^{II}–CO_2^{2-} core, forming a surrounding AM$_3$N$_2$ shell.

In **II** the carbonite ligand is prepared for facile CO elimination, which can be triggered by contact with electrophiles and influenced by the nature of the surrounding Lewis acidic cations AM$^+$ (see Figure 1). Furthermore, for the case of AM=K conditions were found that induce Ni reduction and formation of C–C coupling products.[43]

While correspondingly the Ni^{II} formate/base system can be used as a Ni^0/CO_2 surrogate, the simplicity of a deprotonation reaction with solid precursors (instead of dosing exactly one equivalent of gaseous CO_2) makes this route very convenient for a more detailed analysis of the factors that influence CO_2 activation and the behaviour of the resulting Ni^{II}–CO_2^{2-} species. However, the additional two AM amide equivalents contained in the AM$_3$N$_2$ shell do not stay innocent during reactivity studies of the CO_2 complexes, giving rise to complicated product mixtures.[43]

Herein, we report the synthesis of amide-free mono-metalated complexes [L^{tBu}Ni(CO_2)AM] through replacement of (AM)N(SiMe$_3$)$_2$ by the stronger base (AM)N(^{i}Pr)$_2$. The complexes thus formed turned out to be ideal precursors for further modifications in the second coordination sphere of the Ni^{II}–CO_2^{2-} core. Therefore, a detailed study is presented, showing how distance, number, and nature of the supporting AM cations are affecting the spectroscopic properties and the degree of CO_2 activation at the β-diketiminato nickel site.
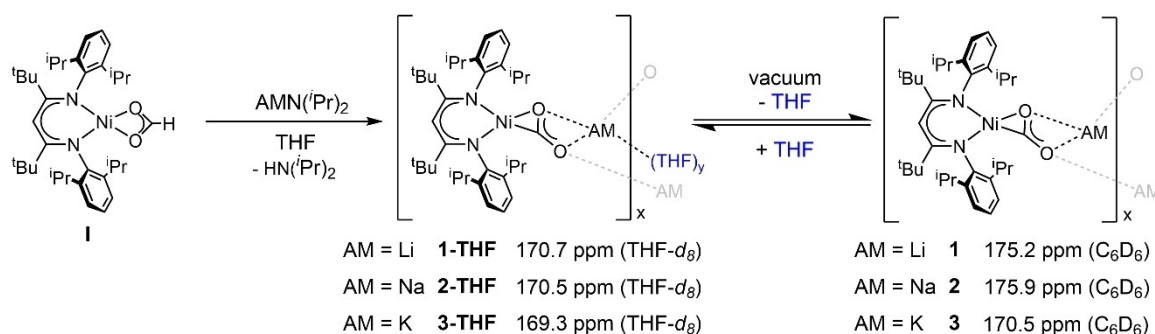
Results and Discussion

Synthesis of mono-metalated complexes

As pointed out above, using (AM)N(SiMe$_3$)$_2$ as a base for the deprotonation it had been found in previous work that three equivalents are required for a clean reaction that leads to an isolable product; the additional two equivalents (beyond the one performing the deprotonation) were then incorporated in the product. However, varying the amide from N(SiMe$_3$)$_2^-$ to N(^{i}Pr)$_2^-$ in the present investigation it turned out that the addition of one equivalent is sufficient for complete deprotonation and formation of products with a Ni/AM ratio of 1:1, namely [L^{tBu}Ni(CO_2)Li(THF)$_x$], **1-THF**, [L^{tBu}Ni(CO_2)Na(THF)$_x$], **2-THF** and [L^{tBu}Ni(CO_2)K(THF)$_x$], **3-THF**. For all three derivatives successful deprotonation of the formate ligand was apparent by a blue shift of the C–O stretching (ν_{CO2}) vibration and a characteristic ^{1}H NMR pattern, resulting from the side-on bound carbonite ligand causing an asymmetric square planar ligand environment around the Ni^{II} ion. Deprotonation studies performed with the ^{13}C-labeled precursor ^{13}**I** enabled monitoring the reactions by ^{13}C NMR spectroscopy and allowed to determine the ^{13}C NMR shifts of the CO_2^{2-} ligand (δ^{13}C$_{CO2}$), characteristic for each derivative (see Scheme 1).

Single crystal X-ray analysis of crystals grown from a saturated hexane solution of **2-THF** confirmed incorporation of only one sodium ion per CO_2 complex. However, it also revealed that in the absence of additional AM amides the complex aggregates to a trimer, (see Figure 2 or SI Figure S12). The sodium ions and the oxygen atoms, distal to the nickel centres, form a Na$_3$O$_3$ core (see Figure 2B). Additional interactions of the Ni-bound oxygen atoms with the sodium ions further stabilise the trimer together with electrostatic interactions between aryl residues and the sodium ions. The determined structure also verified coordination of two THF molecules at the counter ions, one of which adopts a bridging coordination between two Na ions (Figure 2B).

The molecular structure of **3-THF** revealed that also the K derivative exhibits an oligomeric structure (see Figure 3). [L^{tBu}Ni(CO_2)K] entities are arranged in form of polymeric chains in which the [L^{tBu}Ni(CO_2)]$^-$ units are bridged by potassium ions. Thereby each cation binds to the distal oxygen atom of one

Scheme 1. Deprotonation of Ni-formate (**I**) using (AM)N(^{i}Pr)$_2$ to yield mono-metalated carbonite complexes [L^{tBu}Ni(CO_2)AM(THF)$_x$]. Observed ^{13}C NMR shifts (ppm) of the CO_2^{2-} ligands are provided.

AM = Li **1-THF** 170.7 ppm (THF-d_8)   AM = Li **1** 175.2 ppm (C_6D_6)
AM = Na **2-THF** 170.5 ppm (THF-d_8)   AM = Na **2** 175.9 ppm (C_6D_6)
AM = K **3-THF** 169.3 ppm (THF-d_8)   AM = K **3** 170.5 ppm (C_6D_6)

Chemistry–A European Journal

Research Article
doi.org/10.1002/chem.202303112

Chemistry Europe
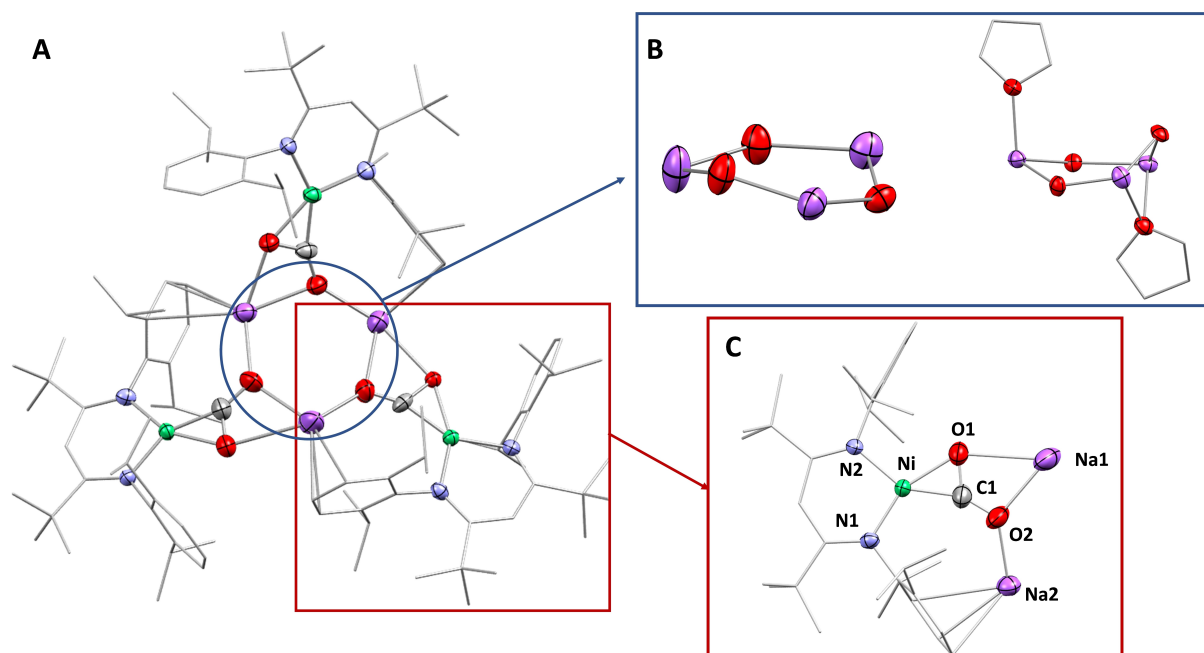European Chemical
Societies Publishing

Figure 2. (A) Molecular structure of **2**. Hydrogen atoms and solvent molecules are omitted for clarity. A similar structural arrangement of the [L^{tBu}Ni(CO$_2$)]Na] moieties was found for the molecular structure of **2-THF** (see SI Figure S12). (B) Comparison of the central Na$_3$O$_3$ core of **2** (left) and **2**-THF (right). (C) Structural section of repeating unit in **2** and **2-THF**. Selected bond lengths [Å] and angles [°] (values are averaged between the three units): **2**: Ni–C1 1.80, Ni–O1 1.96, C1–O1 1.30, C1–O2 1.23; O1–C1–O2 124.5, Na1–O1 2.49, Na1–O2 2.37, Na2–O2 2.18. **2-THF**: Ni–C1 1.80, Ni–O1 1.95, C1–O1 1.29, C1–O2 1.24; O1–C1–O2 127.2, Na1–O1 2.74, Na1–O2 2.37, Na2–O2 2.19.
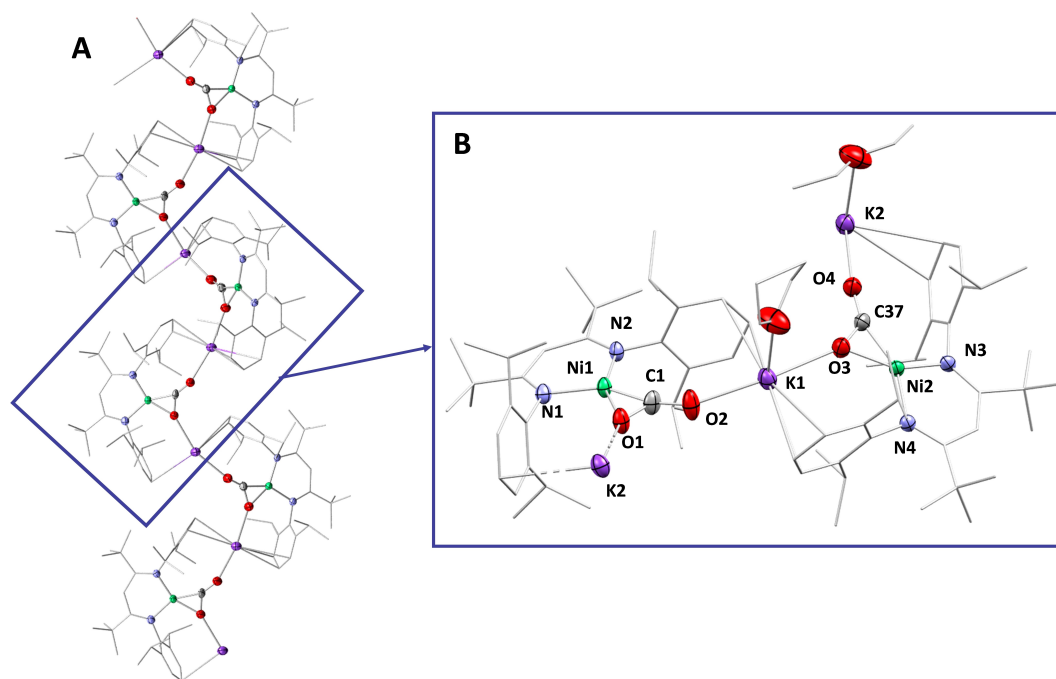

Figure 3. (A) Molecular structure of **(3-THF/Et$_2$O)$_x$**. Hydrogen atoms and solvent molecules (cocrystallised and coordinated) are omitted for clarity. (B) Structural section of the repeating unit. Selected bond lengths [Å] and angles [°]: Ni1–C1 1.805(3), Ni1–O1 1.949(3), C1–O1 1.34(4), C1–O2 1.220(4); O1–C1–O2 130.1(3), K1–O2 2.517(2), K1–O3 2.593(2), Ni2–C37 1.818(3), Ni2–O3 1.932(2), C37–O3 1.298(4), C1–O2 1.222(4); O1–C1–O2 130.3(3), K2–O4 2.599(3), K2–O1 2.632(3).

carbonite ligands as well as to the Ni-bound oxygen atom of the following unit, producing a central [–K–OCO–]$_x$ chain. Furthermore, T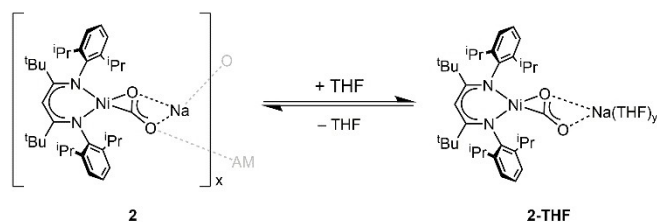HF and Et$_2$O molecules are coordinated to the potassium ions in an alternating fashion yielding an overall composition of [L^{tBu}Ni(CO$_2$)K(THF)L^{tBu}Ni(CO$_2$)K(Et$_2$O)]$_x$, **(3-THF/ Et$_2$O)$_x$** for the single crystalline material; the Et$_2$O donor

Chemistry–A European Journal

Research Article
doi.org/10.1002/chem.202303112

Chemistry
Europe
European Chemical
Societies Publishing

molecules originate from the solvent mixture used for crystallisation and they are not present directly after synthesis of **3-THF** in pure THF.

Although numerous attempts to grow crystals of **1-THF** were carried out, this compound eluded crystallisation, preventing determination of its structure in the solid state. However, based on the data collected for the heavier analogues it is reasonable to assume that also **1-THF** exhibits an oligomeric structure.

It was found that coordinated THF can be removed from the AM ions by applying several drying cycles under vacuum. This gave rise to the donor-free variants [L^{tBu}Ni(CO$_2$)]AM], **1**, **2** and **3** (see Scheme 1). While no single crystalline material could be obtained in case of **1** or **3**, X-ray analysis of single crystals of **2**, grown from a saturated benzene solution, revealed that the trimeric structure remains conserved upon removal of coordinated THF (see Figure 2 and Figure S11). The molecular structure of **2** essentially matches the one of **2-THF**, except that the Na$_3$O$_3$ ring adopts an almost planar conformation while for **2-THF** a boat-like arrangement has been observed (see Figure 2B). While the structures of **2** and **2-THF** in the crystalline state indicate that THF coordination at the AM ions does not affect the oligomeric constitution of molecules in the solid state, the question arose whether this is also true in solution. Therefore, diffusion ordered spectroscopy (DOSY) NMR measurements were conducted which confirmed the oligomeric nature of **2** in non-coordinating solvents (see SI section 4). However, based on the determined diffusion coefficients the size of the oligomer could not be estimated with sufficient certainty. In contrast, measurements performed in THF solutions indicate that **2-THF** exists as monomer in this solvent. Hence, the determined solid-state structure of **2-THF** does not reflect the true constitution of the molecule in solution but represents the favourable arrangement in the crystalline state. In the presence of excessive THF molecules these cleave the contacts between the sodium ions to neighbouring carbonite units thus leading to a breakdown of the oligomers (see Scheme 2).
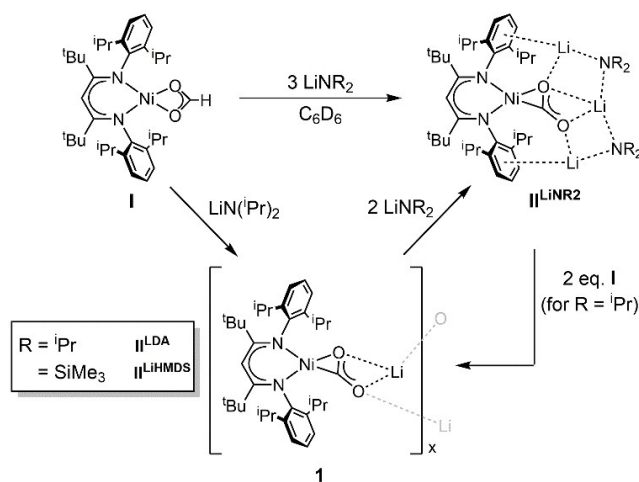
Having found that the use of (AM)N(^{i}Pr)$_2$ as a base allows isolation of complexes with Ni/AM ratios of 1:1, the question arose why deprotonation with (AM)N(SiMe$_3$)$_2$ required three equivalents leading to complexes **II** with Ni/AM ratios of 1:3. Seeking for an answer, ^{13}**I** was reacted with varying amounts of LiN(^{i}Pr)$_2$. While reaction with just one equivalent of base in C$_6$D$_6$ gave **1**, as indicated by the occurrence of a single resonance in the ^{13}C NMR spectrum, reaction with two equivalents caused the formation of a product mixture containing **1** and another

new species with a $\delta^{13}C_{CO_2}$ of 174.1 ppm. After adding a third equivalent of LiN(^{i}Pr)$_2$ the signal of **1** was not observable anymore while the new signal prevailed, indicating formation of a single product. Based on the ^{1}H NMR spectrum in combination with IR spectroscopic analysis it was concluded that the new species corresponds to [L^{tBu}Ni(CO$_2$)]Li$_3$[N(^{i}Pr)$_2$]$_2$, **II^{LDA}**, which forms in a stepwise fashion involving **1** as an intermediate (see Scheme 3). Therefore, we tested whether **1** can also be converted into **II^{LiHMDS}** by addition of two equivalents of LiN(SiMe$_3$)$_2$. Indeed, formation of **II^{LiHMDS}** could be verified by NMR and IR spectroscopy. Hence, **1** can be employed as a precursor for various complexes of type [L^{tBu}Ni(CO$_2$)]Li$_3$[NR$_2$]$_2$, regardless of the coordinated amide. This is surprising, since intermediate formation of **1** had never been observed for reactions of **I** with LiN(SiMe$_3$)$_2$.[41] Using less than three equivalent of LiN(SiMe$_3$)$_2$ leads to an incomplete conversion of **I** to **II^{LiHMDS}** as well as to some undesired side reactions. To ascertain whether the deprotonation product for each base arises from kinetic or thermodynamic control test reactions between the amide adducts and **I** were performed. Interestingly, the reaction of **II^{LDA}** with two equivalents of **I** led to the formation of **1** via deprotonation of the formate ligands by the co-coordinated amide functions. Such transformation could not be observed when **II^{LiHMDS}** was reacted with **I**. Apparently, the higher basicity of LiN(^{i}Pr)$_2$ favours the deprotonation of the formate ligand such that **1** becomes accessible, while for LiHMDS adduct formation is favoured.

Also for **2** and **3** it was proven that the complexes can act as precursors for their analogues with two additional (AM)NR$_2$ equivalents incorporated (see Scheme 4). Applying such a stepwise synthetic approach with initial generation of **3** enabled the isolation of **II^{KHMDS}** and determination of its molecular structure, which had not been possible in previous attempts using KN(SiMe$_3$)$_2$ directly.[41,43] The obtained data of **II^{KHMDS}** confirmed that the K$_3$N$_2$ shell is bent out of the (N)$_2$Ni(CO$_2$)-plane (see SI Figure S30), as was previously predicted by DFT calculations.[43]
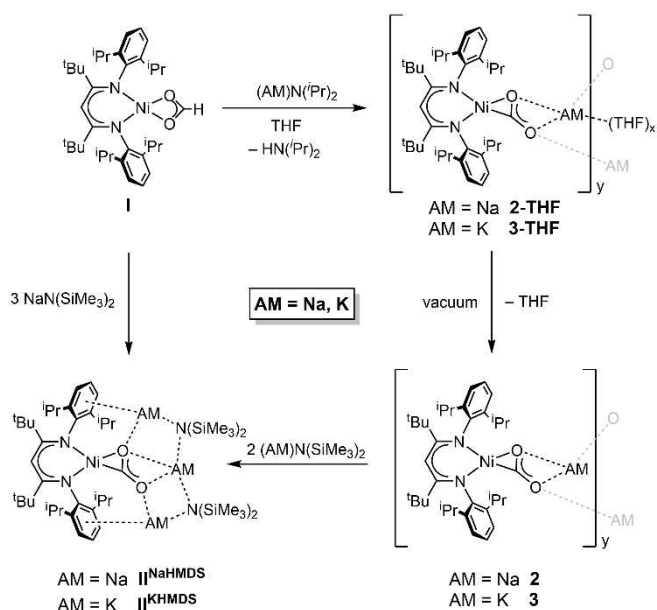

Scheme 2. Interconversion of oligomeric **2**, observed in non-coordinating solvents (left), and monomeric **2-THF** observed in solution of THF (right).

Scheme 3. Stepwise synthesis of complexes **II^{LiNR2}**, involving **1** as the intermediate.

Scheme 4. Stepwise synthesis of complexes II$^{(AM)HMDS}$ (AM=Na, K), involving **2** or **3** as the intermediate.

The results presented so far may be summarised as follows: Obviously, once generated with (AM)N(^{i}Pr)$_2$ as the base the complexes **1–3** feature Lewis acidic character at the AM counterion. Accordingly, in the absence of donor molecules the AM ions saturate their coordination sphere by using donor atoms from neighbouring molecules, which leads to oligomerisation. Addition of amides yields monomeric complexes of type **II** stabilised by a surrounding AM$_3$N$_2$ shell. Similarly, when formate deprotonation is performed in THF, coordination of solvent molecules occurs giving rise to donor adducts **1-THF**, **2-THF** and **3-THF**, which exhibit a monomeric nature in solution. However, THF binding is reversible such that oligomeric arrangements are accessible, which preferably crystallise.

Having identified the constitution of the compounds in the solid state and in solution as well as their interconversion, a closer look at the nickel carbonite moieties will be taken next. The spectroscopic data of the complexes suggest that coordination of the solvent molecules is not just affecting the aggregation behaviour but also the electronic situation of the Ni–CO$_2$$^{2-}$ core. Comparing **1** and **2** with their respective THF adducts **1-THF** and **2-THF** δ^{13}C$_{CO_2}$ values shift upfield by around 5 ppm upon coordination of THF. A NMR titration experiment (see SI Figure S5 and S6) for which THF was added in portions to a C$_6$D$_6$ solution of **1** proved that the upfield shift indeed arises from THF coordination at the lithium centre to form **1-THF** and is not just originating from the different solvent system. Interestingly, for K derivatives **3** and **3-THF** spectroscopic differences were less pronounced indicating that the Ni–CO$_2$–K core is less affected by THF coordination at the potassium ion (see Scheme 1 for δ^{13}C$_{CO_2}$ data or SI Table S2).

In order to find the origin of these spectroscopic changes, the bond parameters for **2** and **2-THF** were compared (see Figure 2 or SI Table S2). Upon THF coordination only slight

structural changes were observed within the CO$_2$$^{2-}$ ligand. Interestingly, the distance between the Ni-bound oxygen atom and the sodium ion (O1–Na1) got significantly elongated by about 0.2 Å upon THF coordination (see Figure 2C). This indicates that coordination of donors at the AM induces its detachment and thereby weakens the interaction of the Lewis acidic counterion with the CO$_2$$^{2-}$ ligand. Due to the lack of structural information for **1** and **3** no general claim can be made. However, the influence of coordinating donor moieties on the CO$_2$ activation will be further investigated in the following.

Variation of the ligand support – alkali metal detachment

The tendency of anionic complexes with AM counterions to form oligomers is a well-known phenomenon.[44–46] Typically, the size of the oligomers can be controlled by the addition of donor ligands which saturate the coordination sphere of the AM ions and thereby prevent bridging arrangements. In this context, chelating ligands, such as macrocyclic crown ethers or polycyclic cryptands, have been proven very efficient as they can cause a breakdown of oligomers yielding monomeric compounds or even separated ion pairs.[47] Previous reports have also shown that addition of crown ethers to transition metal CO$_2$ complexes featuring AM counter ions allows for the isolation of well-defined monomeric compounds.[42,48] Accordingly, the experiments discussed throughout the previous section have shown that coordination of donor molecules like THF towards the AM counterion is affecting the constitution of the oligomeric complexes **1–3**, especially in solution. Furthermore, the spectroscopic data suggests that the presence of THF is affecting the binding situation around the Ni^{II}–CO$_2$$^{2-}$ core, indicating that THF coordination around the AM is altering its interaction with the carbonite ligand. However, the lability of the THF ligands impede a more comprehensive examination on how [AM(THF)$_x$]$^+$ entities influence the Ni-mediated CO$_2$ activation. Therefore, THF was replaced by chelating ligands to afford a series of complexes with well-defined ligand to metal ratios (see Figure 4). These complexes of type [L^{tBu}Ni(CO$_2$)]AM-(ligand)$_x$] (x = 1, 2) were synthesised via reaction of the AM derivatives **1**, **2** or **3**, generated in situ prior to use, with the respective ligand in non-coordinating solvents (see Scheme 5). Purification of the resulting products was significantly simplified compared to the donor free derivatives since the solubility of the complexes in non-polar solvents was drastically decreased,
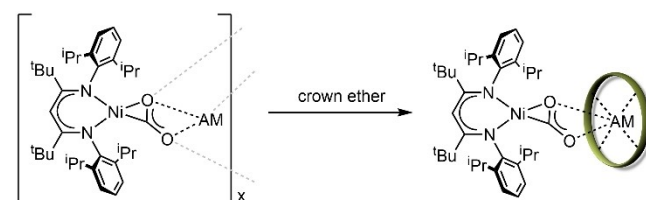
Scheme 5. General scheme for the formation of monomeric AM carbonite complexes supported by polyether ligands.
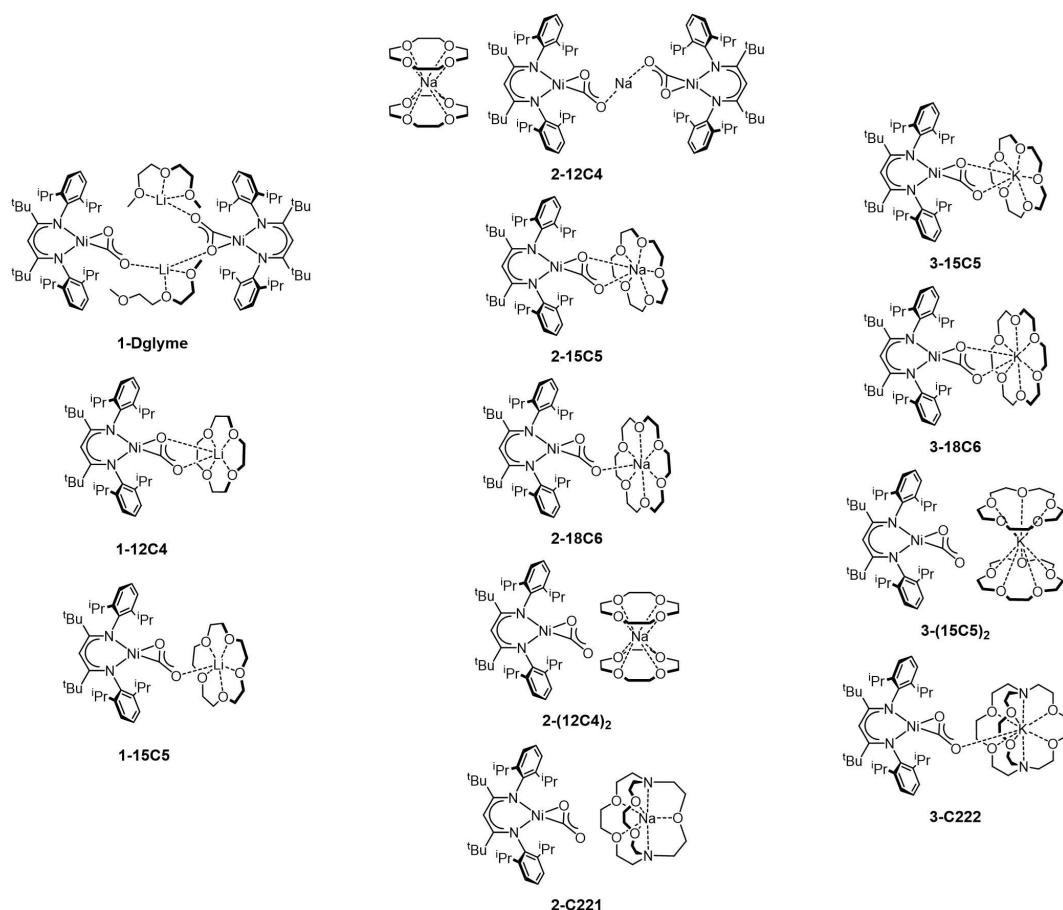
Chemistry–A European Journal

Research Article
doi.org/10.1002/chem.202303112

Chemistry Europe
European Chemical
Societies Publishing

Figure 4. Overview for all synthesised complexes of type [L^{tBu}Ni(CO$_2$)]AM(ligand)$_x$ (x = 1, 2). The drawn structures were determined by single crystal X-ray analysis.

enabling simple precipitation of the clean product from hexane. The molecular structures of most presented complexes were determined by single crystal X-ray analysis, allowing to monitor the structural changes around the Ni^{II}–CO$_2^{2-}$–AM core upon ligand variation.

Reaction of **1** with diglyme afforded **1-Diglyme** and thus the first structurally characterised mono-lithiated derivative of the presented complexes. **1-Diglyme** features a 1:1 ratio between the Li$^+$ counter ion and the coordinated glycol chain, which, unlike THF, could not be removed from the complex under vacuum. Although DOSY measurements indicated a monomeric constitution in solution (see SI section 4) the determined structure still revealed that **1-Diglyme** forms a dimer in solid-state, in which one of the Li$^+$ counterions connects two CO$_2^{2-}$ ligands (see SI Figure S40). Notably, this bridging lithium ion is only coordinated in a η^2-fashion by its diglyme ligand, so that one ether donor remains dangling, while the non-bridging ion is fully coordinated by its diglyme ligand. Apparently, this flexibility in coordination of the linear glycol chain allows the favourable formation of the dimer in the crystalline state. Hence, **1** was reacted with cyclic crown ethers which due their macrocyclic effect bind the ions more strongly. Indeed, reaction with 12-crown-4 afforded the monomeric complex **1–12C4** in which the CO$_2^{2-}$ ligand adopts a η^2-κ^{2}O,O′

coordination towards the lithium ion. Interestingly, when **1** was instead reacted with the larger crown ether 15-crown-5 the resulting complex **1-15C5** was also isolated as a monomeric species, however, the coordination mode of the carbonite ligand at the lithium ion changed from η^2-κ^{2}O,O′ to η^1-κO. Comparison of both structures (see Figure 5) revealed that in **1–12C4** the lithium ion is located out of the cavity allowing interaction with both carbonite oxygen atoms, while in **1-15C5** the ion is much more embedded in the crown ether cavity and therefore only allows interaction with the sterically accessible distal oxygen atom.
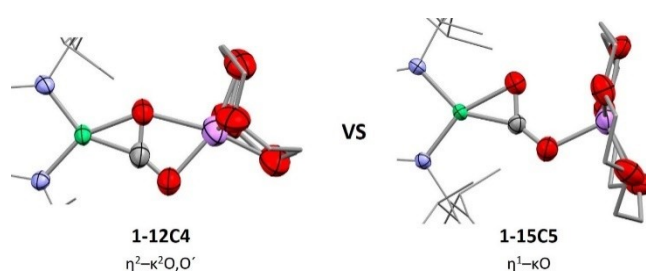

Figure 5. Comparison of the Li$^+$–CO$_2^{2-}$ bonding mode between **1–12C4** and **1-15C5**.

Chemistry–A European Journal

Research Article
doi.org/10.1002/chem.202303112

Chemistry Europe
European Chemical
Societies Publishing

Having found that the size and structure of the co-ligand support is affecting the coordination of the AM ion quite drastically also the heavier homologues **2** and **3** were reacted with crown ethers of varying size. Reaction of **2** with either 15-crown-5 or 18-crown-6 gave rise to **2-15C5** and **2-18C6** which compared to each other display a similar change in the coordination mode of the AM ion as the lithium analogues upon increase of the ligand size. Synthesis of **3–18C6**, which shares the same $\eta^2\text{-}\kappa^2O,O'$ coordination as **1–12C4** and **2-15C5**, has been previously described by Hayton et al.[42] starting from CO_2, but could also be achieved in the course of this investigation via the formate deprotonation route. When **2** or **3** were instead reacted with crown ethers, which are too small to host the ions within its cavity two derivatives with varying amounts of crown ether were isolated. Reaction of **2** with 12-crown-4 afforded the dinickel compound **2-12C4**. Although the complex features an overall AM/crown ether ratio of 1:1 this does not emerge locally: one of the sodium ions is encapsulated by two 12-crown-4 molecules to yield a separated $[Na(12C4)_2]^+$ ion while the second one is bridging two CO_2^{2-} ligands to give the corresponding $[(L^{tBu}NiCO_2)_2Na]^-$ counterion. Apparently, the four oxygen donors of 12-crown-4 are not sufficient to stabilise a monomeric constitution of **2–12C4** and therefore this ionic arrangement is favourable. DOSY measurements confirmed that the dinuclear structure with a separated $[Na(12C4)_2]^+$ ion remains preserved in solution (see SI section 4). Addition of a second equivalent of 12-crown-4 leads to the encapsulation of the second sodium ion to afford the monomeric complex **2-(12C4)_2**. The molecular structure indicated the formation of a separated ion pair in which no interaction between the carbonite and sodium ion was present anymore. Also, for the reaction between **3** and 15-crown-5 formation of the two complexes **3–15C5** and **3-(15C5)_2** was observed which behave almost like ionic liquids as they tend to separate as a viscous oil from solution. This prevented structural characterisation since no single crystalline material was obtained. Assuming that encapsulation of the potassium ion in **3-(15C5)_2** also leads to the

formation of a separated ion pair it was expected that **2-(12C4)_2** and **3-(15C5)_2** provide the same spectroscopic features in regard to the $Ni^{II}\text{-}CO_2^{2-}$ core as both derivates exhibit an isolated $[L^{tBu}Ni(CO_2)]^-$ ion. Surprisingly, the $\delta^{13}C_{CO2}$ values and ν_{CO2} frequencies were somewhat different for both compounds, suggesting that the situation is more dynamic in solution. Consistently, we observed that addition of further equivalents of 12-crown-4 to **2-(12C4)_2** causes the $\delta^{13}C_{CO2}$ value to shift further upfield indicating that in solution interaction between the cation and the carbonite ligand does occur (see SI Figure S83).

To further examine this finding, we exchanged the crown ethers by even more chelating cryptands, capable of encapsulating AM ions. Reaction of **2** with 4,7,13,16,21-Pentaoxa-1,10-diazabicyclo[8.8.5]tricosane (**C221**) yielded **2-C221** which was found to crystallise in two different solid-state structures depending on the chosen conditions (see Figure 6). While slow crystallisation from toluene at low temperatures afforded crystals of the compound with a separated ion pair structure, fast crystallisation by evaporation of a hexane/Et₂O mixture gave rise to crystals corresponding to a structure, in which the distal oxygen atom remains coordinated to the sodium ion (**2-C221′**). For the corresponding derivative **3-C222**, derived from reaction of **3** with 4,7,13,16,21,24-hexaoxa-1,10-diazabicyclo[8.8.8]hexacosane (**C222**), the molecular structure also showed interaction between the potassium ion and carbonite (see SI Figure S98). Further attempts to grow crystals of a structural isomer without interaction were not undertaken.

The findings show that the solid-state structures of the complexes presented here do not necessarily reflect their true nature in solution. This is in line with the situation of **2-THF**, for which, as outlined before, DOSY measurements suggest the presence of monomers in THF solutions, while it assembles into a trimer during crystallisation. Nevertheless, the determined molecular structures represent minima on the potential energy surface, which should be highly relevant also in solution and they reflect how the interaction strength between the CO_2^{2-}
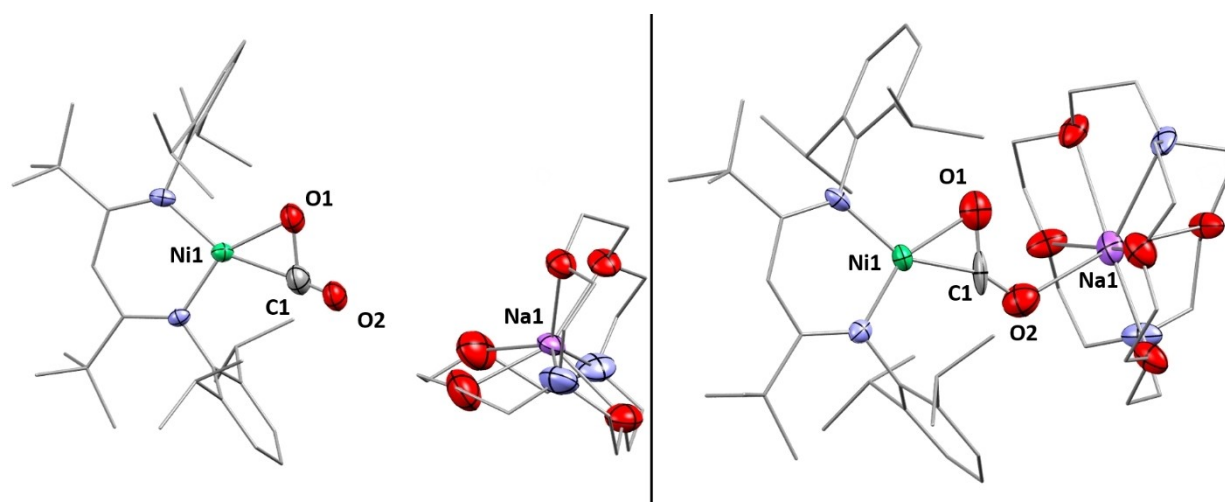

Figure 6. Molecular structures of the two isomers of **2-C221**. Left: Separated ion pair structure. Right: Structure which features interaction of the carbonite ligand with the sodium counterion (**2-C221′**).

Chemistry–A European Journal

Research Article
doi.org/10.1002/chem.202303112

Chemistry Europe
European Chemical
Societies Publishing

ligand and its counter ion evolves upon variation of the co-ligand. For ligands with a low number of coordinating sites a strong contact between the AM and CO_2^{2-} ligand is observed even allowing intermolecular interaction. However, with increasing number of chelating donor sites inherent to the ligand support the host-guest affinity towards the AM is also increased which induces a detachment from the CO_2^{2-} ligand. Based on the extent of collected data one can see that this detachment occurs stepwise, starting with breakdown of oligomers until a complete ion separation is achieved (see Figure 7).

Notably, cleavage of the CO_2^{2-}-AM interaction to form separated ions was only achieved for the heavier AM analogues while attempts to isolate a corresponding lithium derivative failed. Reaction of **1** with larger crown ethers or cryptands did not lead to a detachment of the counterion as it was only partially coordinated by the co-ligand. Apparently, the interaction of lithium towards the carbonite ligand is too strong to be compensated by the host-guest interaction.

The presented complexes do not only differ by their solid-state structures but are also distinguished by their $\delta^{13}C_{CO2}$ values and ν_{CO2} frequencies, showing that the AM detachment affects the bonding situation of the $Ni^{II}-CO_2^{2-}$ unit and thereby also the "degree of CO_2 activation".

Degree of activation of CO$_2$

Due to its ambiphilic nature, resulting from the presence of an electrophilic carbon atom as well as nucleophilic oxygen atoms, CO_2 is highly eligible for bifunctional activation processes. While this property is extensively exploited by FLP-type systems,[49–52] also transition metal based activation benefits from combination of Lewis acidic and Lewis basic sites. Although binding of CO_2 at a single Lewis basic metal is generally possible,[52–56] supporting interaction with Lewis acids facilitates the $M{\rightarrow}CO_2$ electron transfer and stabilises the resulting charge distribution at the molecule.[23,25,34,56–60] As a consequence, bifunctional systems usually allow for a stronger binding of the CO_2 ligand and a higher degree of activation, referring to a stronger donation of electron density into the antibonding orbitals of the molecule. The latter usually translates into structural changes for the CO_2 ligand, as for example bending of the linear molecule or elongation of the C—O bonds. The latter is also reflected by a red shift of the ν_{CO2} bands. For diamagnetic systems also $\delta^{13}C_{CO2}$ values can be used to describe the degree of activation. While changes of ν_{CO2} frequencies as well as structural deformation of the CO_2 ligand are consequences of the occupation of antibonding orbitals, the relation between
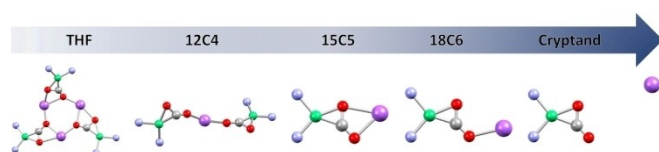
the degree of activation and $\delta^{13}C_{CO2}$ values is not as clear. However, the results of empirical studies suggest that stronger activation is usually accompanied by downfield shifts. Preceding work of Agapie et al. has demonstrated that the degree of activation, as indicated by IR and ^{13}C NMR spectroscopic data, of a Mo^0-bound CO_2 ligand correlates with the strength of the cooperating Lewis acid.[61] The question still remains whether this relation is also applicable to other systems and which further factors may affect the degree of CO_2 activation.

Also, in the complexes described here CO_2 is activated in a cooperative fashion between the electron donating nickel centre and the Lewis acidic AM counterion. So far, this study has shown that the mono-metalated complexes **1**, **2** and **3** offer an excellent platform for modifications in the second coordination sphere around the $Ni^{II}-CO_2^{2-}$ core. As demonstrated, the following three parameters can be easily modified by simple adjustment during synthesis:

(1) the nature of the cooperating Lewis acidic AM counter ion,
(2) the number of Lewis acidic and Lewis basic centres in the second coordination sphere (AM_3N_2 shell),
(3) the distance between the CO_2^{2-} ligand and the cooperating Lewis acid.

During the following section, a discussion concerning the relevance of these parameters on the CO_2 activation will be given based on the structural and spectroscopic database provided throughout this study (the discussed data are summarised in SI section 3).

AM variation

With increasing atomic number, the AMs become softer and lose their oxophilic character leading to a decrease in Lewis acidity. Hence, upon variation of the AM counterion it is expected that strongest activation of the carbonite ligand is reached by the lithium derivatives while for the sodium and potassium analogues a gradual decrease in activation should be observed. This assumption was indeed supported by the IR and NMR spectroscopic data of the presented complexes. When comparing AM derivatives of similar constitution, a general blue shift of the ν_{CO2} bands and an upfield shift of the $\delta^{13}C_{CO2}$ values were observed on moving from the lighter to the heavier AM ions. Both trends are indeed indicative for a weakening of activation in order $Li > Na > K$ (data is summarised and graphically presented in SI section 3.1).

To further support this finding evolution of the metric data around the $Ni^{II}-CO_2^{2-}$ core was examined for the derivatives **1–12C4**, **2-15C5** and **3–18C6** (see Figure 8 and SI Table S1, bottom row). It is observed that the CO_2 bond angles decrease upon transition from potassium to lithium, accompanied by an elongation of the side-on coordinated C—O bond (C1—O1). Both trends support the conclusion that the degree of activation correlates with the Lewis acidity of the counter ion. However, comparison of the lengths for the distal C—O bonds (C1—O2) indicates an inverse trend, as the bond is gradually contracted upon transition from K to Li. Counterintuitively, this suggests a strengthening of the bond while the overall molecule is more
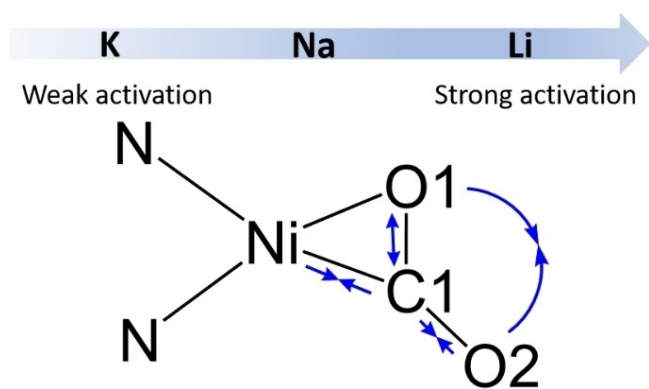

Figure 7. Structural development of the $Ni^{II}-CO_2^{2-}-AM$ core upon variation of ether ligand support (exemplified on the series of sodium derivatives).

Chemistry–A European Journal

Research Article
doi.org/10.1002/chem.202303112

Chemistry Europe
European Chemical
Societies Publishing

Figure 8. Structural evolution of the Ni^{II}–CO_2^{2-} core upon AM variation.

Figure 9. Selected sets of complexes for comparison of the spectroscopic features to access the influence of the AM_3N_2 shell on the CO_2 activation.

activated. Apparently, increasing activation of the CO_2 molecule at the nickel site leads to an increasing divergence of both C–O bonds which is indeed consistently observed across all presented complexes. Considering that upon binding between the Ni–AM site the CO_2 molecule is prepared for a C–O bond cleavage the structural evolution of the carbonite unit with increasing activation may be regarded as a prearrangement of this step.

Apart from the metric changes within the CO_2^{2-} ligand itself, also the binding towards the nickel centre, namely the Ni–C1 bond, was considered for evaluation. Interestingly, it was observed that this bond experiences a contraction in the order K > Na > Li. Since CO_2 activation proceeds in a kind of push-pull interaction, the increased Lewis acidity of the lighter AM ion facilitates the electron transfer from the nickel to the carbon atom leading to a strengthening of the Ni–C1 bond for higher degrees of activation.

Multi-functional activation

Transformation of **1**, **2** or **3** into the respective complex **II** is accompanied by an accumulation of two additional AM cations around the Ni^{II}–CO_2^{2-} core. Due to the contact with three Lewis acidic centres, one would assume that complexes **II** feature a higher degree of CO_2 activation compared to their mono AM analogues. To examine whether this assumption is valid, spectroscopic data of the two types of complexes were compared for each of the AM ions (see Figure 9A).

Upon formation of the AM_3N_2 shell the C–O stretching frequencies of the carbonite ligand experience a general red shift (see Figure 10A,B and C and Table S3), indicating that indeed each derivative of **II** features a stronger CO_2 activation than its corresponding mono AM analogue. This trend was also supported by the evolution of $\delta^{13}C_{CO_2}$ values for **1** and **II^{LiHMDS}** (175.2 ppm vs. 177.6 ppm) showing a downfield shift upon accumulation of two further Li^+ ions around the carbonite ligand. Contrary to this, the $\delta^{13}C_{CO_2}$ values for **II^{NaHMDS}** and **II^{KHMDS}** suggest that the CO_2 unit in the complexes experiences a lower degree of activation than their analogues **2** (173.2 ppm vs.
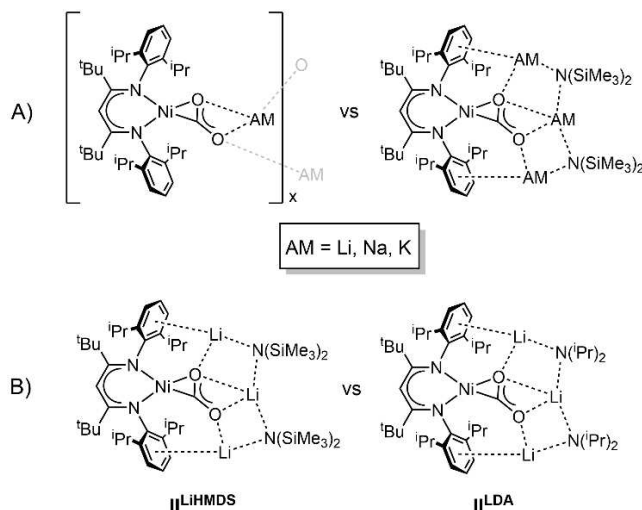
175.9 ppm) and **3** (169.5 ppm vs. 170.6 ppm). This can be understood as follows:

Undeniably, the spectroscopic data indicate that in the entire series of complexes the extent of CO_2 activation is largest in **II^{LiHMDS}**, since it features the highest $\delta^{13}C_{CO_2}$ value, the lowest ν_{CO_2} frequency and the shortest Ni–C1 bond. Hence, it appears that coordination of additional AM amide equivalents favours CO_2 activation especially in case of AM=Li, whereas this effect seems to be less pronounced for sodium and potassium. This phenomenon can be rationalized by the high oxophilicity of Li^+, which is thus prone to strongly interact with the CO_2^{2-} ligand. In case of the softer cations Na^+ and K^+ interactions with the bridging $[N(SiMe_3)_2]^-$ moieties become stronger and therefore quench the interaction with the CO_2^{2-} ligand.

In order to verify the assumption that the bridging amides have an influence as well, NMR and IR data of **II^{LiHMDS}** and **II^{LDA}** were compared (see Figure 9B). Due to the increased +I effect, the bridging $[N(^iPr)_2]^-$ moiety is a stronger electron donor, which should to some extent quench the interaction of the Li^+ ions with the CO_2^{2-} ligand. Indeed, the ν_{CO_2} band of **II^{LDA}** appears at a higher frequency (see Figure 10D) and at the same time a lower $\delta^{13}C_{CO_2}$ shift compared to **II^{LiHMDS}** (177.6 ppm vs. 174.1 ppm) is observed, conterminous with a decrease of CO_2 activation. This emphasises that construction of the AM_3N_2 shell leads to a multi-functional system, and to ascertain the influence it exerts on the Ni^{II}–CO_2^{2-} unit in comparison with mono metalated complexes it has to be considered as a whole, including the increased number and the nature of AM ions as well as the bridging amide entities.

Spatial separation

As already discussed throughout the previous section, increasing the size of the chelating polyether co-ligand leads to a progressing detachment of the counterion from the carbonite
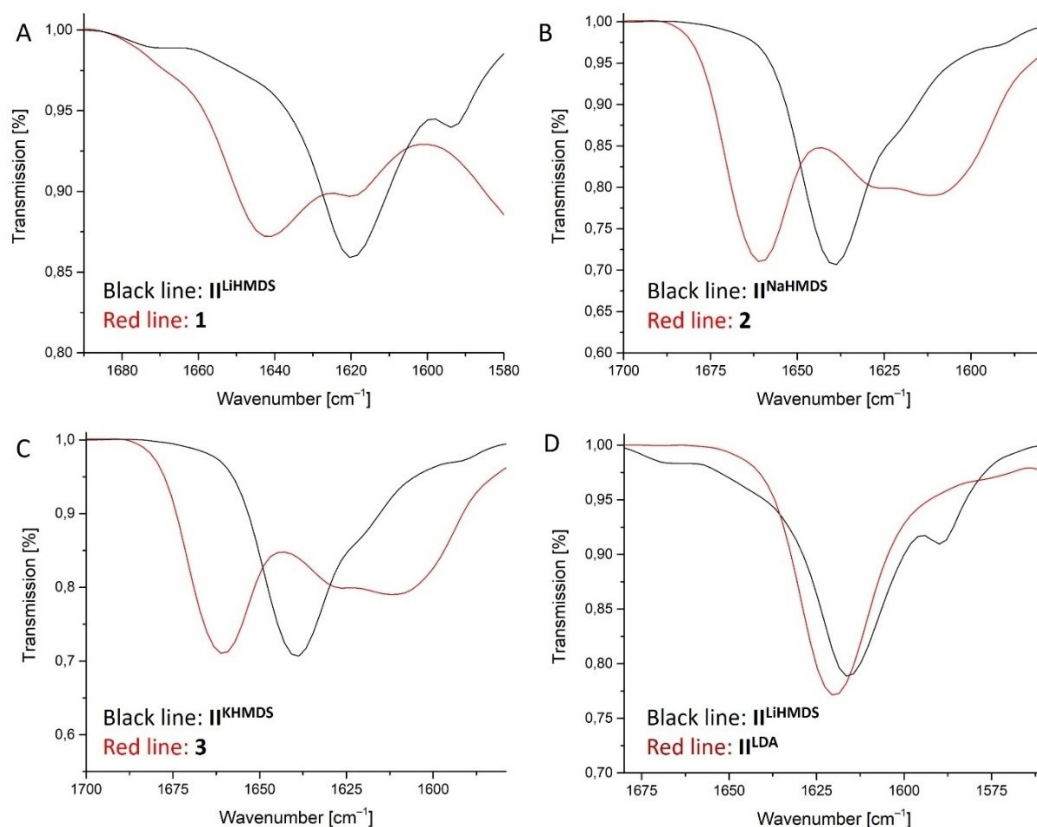
Chemistry–A European Journal

Research Article
doi.org/10.1002/chem.202303112

Chemistry
Europe
European Chemical
Societies Publishing

Figure 10. Comparison of the ν_{CO_2} band for complexes **1**–**3** with the respective derivative of type **II** (A,B,C) and comparison between **II**^{LiHMDS} and **II**^{LDA}.

in the crystalline state (see Figure 7). Since the spatial separation between cooperating sites leads to a quenching of the push-pull interaction through the carbonite ligand, it is expected that CO_2 activation is weakened. This is indeed supported by a continuous high-field shift of the $\delta^{13}C_{CO_2}$ value for each group of AM derivatives with progressing cation detachment (see Figure 11 and SI Table S2). This was consistent across all presented complexes without any exceptions. The decrease in activation was also displayed by a general blue shift of ν_{CO_2} frequencies although some outliers were found in the data set (IR data is summarised and graphically presented in SI section 3.1). The combined spectroscopic data therefore clearly shows that cleavage of CO_2^{2-} AM contact leads to a decrease in CO_2 activation.

Concluding remarks to the observed trends

It has been shown that chemical and structural modifications of the second coordination sphere around the Ni^{II}–CO_2^{2-} core have a notable effect on its spectroscopic features which are direct measures for the degree of CO_2 activation. Each modification can be tuned individually but the evaluation has shown that overall the nature of the AM counterion has the strongest influence. Construction of an AM_3N_2 shell turned out to further support CO_2 activation especially in case of hard oxophilic counterions. AM detachment could be achieved most
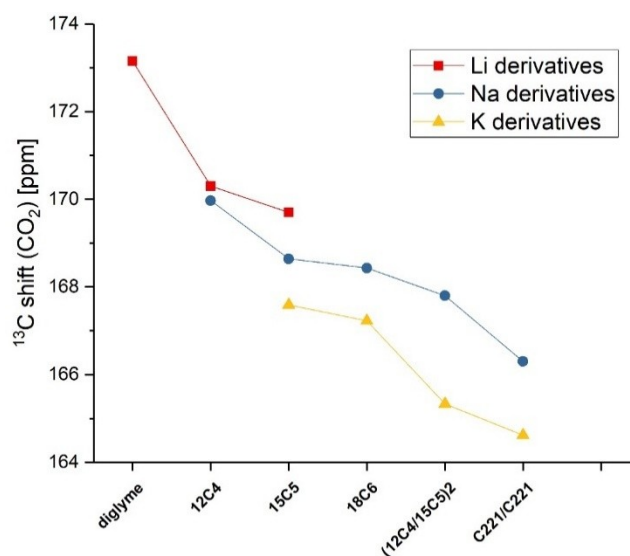

Figure 11. Graphic plot of $\delta^{13}C_{CO_2}$ values against co-ligands with rising number of O-donor functions (to the right) that lead to an increasingly pronounced detachment of the AM ions from the carbonite entity in the complexes shown in Figure 4.

readily for soft AM derivatives, which feature weaker interaction towards the carbonite.

These trends are best illustrated when comparing both extremes in terms of activation. **II**^{LiHMDS} exhibits the strongest activation of the carbonite ligand due to the presence of three

Chemistry–A European Journal

Research Article
doi.org/10.1002/chem.202303112

Chemistry
Europe
European Chemical
Societies Publishing

lithium ions which favour strong donation of electron density into the antibonding orbitals of CO_2. In contrast, for **3-(15C5)$_2$** and **3-C222** interaction of the soft potassium counterion with the Ni^{II}–CO_2^{2-} core is strongly weakened due to the spatial separation induced by the donor-rich macrocycles leading to the weakest activation of the CO_2^{2-} ligand. Hence, the combination of all three discussed modifications of the second coordination sphere allows a very modular and tuneable control of CO_2 activation.

Computational study on ν_{CO_2} and $\delta^{13}C_{CO_2}$ values

In the previous section, general assessment of the degree of CO_2 activation was based on a combined evaluation of NMR, IR and XRD data. Changes of the C–O vibrations or the metric parameters around the carbonite ligand are direct consequences of the population of the anti-bonding orbitals and are therefore good measures for interpretation. However, to date no explanation on the relation between the $\delta^{13}C_{CO_2}$ value and the degree of CO_2 activation has been given in the literature. Therefore, five complexes II^{LiHMDS}, II^{NaHMDS}, **1–12C4**, **1–15C5**, and **2–15C5** were selected for our computational study at the TPSSh-D3(BJ)/dev2-TZVP/IEFPCM(toluene) hybrid DFT level (see Computational Details in Supporting Information). As shown in Figure S136, DFT optimisation indicates that structures of these five complexes remain largely consistent with their X-ray references, suggesting a small influence of crystal packing effects. Notably, this pertains also to the positioning of the variable 2nd- and 3rd-shell ligands to the Ni center beyond η^2-CO_2, which lack covalent bonds to the invariable $L^{tBu}Ni$ fragment shared by all the complexes. The DFT-optimized $Ni(\eta^2$-$CO_2)$ moiety displayed only a small variation within 0.02 Å in either Ni–C or C–O bonding distances (Table S6) and within 3° in the OCO angle, among the five complexes studied. The shortest Ni–C1 and longest C1–O2 and *vice versa*, longest Ni–C1 and shortest C1–O2 bonds (as designated in Figure 8) within the set were received for complexes II^{LiHMDS} and **2–15C5** correspondingly.

Interestingly, our DFT analysis of the ν_{CO_2} modes revealed a low-energy vibration in the ~1100–1200 cm^{-1} region, which is mostly a C–O1 stretch admixed with C/N nuclei motion in the L^{tBu} ligand, as shown e.g. for II^{LiHMDS} in Figure S143. The corresponding ν_{C-O1} fingerprints in the experimental ATR-IR spectra have been identified, facilitated by red shifts in the bands of the $^{13}CO_2$-labelled species (Figures S138–S142). Furthermore, the well-resolved ν_{CO_2} IR features in the ~1600–1700 cm^{-1} region, commonly referred to as resulting from the asymmetric C–O1/O2 stretch, were now disclosed to bear predominantly C–O2 character (Figure S143) with only a minor component of C–O1. The relative position of the ν_{C-O1} and ν_{C-O2} frequencies correlates well with longer C–O1 and shorter C–O2 bonds of the Ni-bound CO_2 (see e.g. Table S6). Among the complexes computed, II^{LiHMDS} stands out displaying the highest ν_{C-O1} and lowest ν_{C-O2} frequencies consistently from ATR-IR and DFT (Figure S138). This goes in line with II^{LiHMDS} providing an extreme on the $Ni(\eta^2$-$CO_2)$ moiety structure (*vide supra*), as well

as η^2-CO_2 charge and $\delta^{13}C_{CO_2}$ shift (*vide infra*). Notably, spectral shoulders observed in the higher energy ν_{C-O1} bands could not be reproduced by computations. They will have their origins in sub-conformers of the same species present in the solid-state samples.
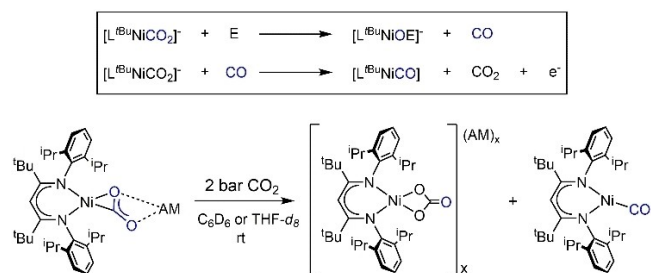
To carry out relativistic DFT calculations of the $\delta^{13}C_{CO_2}$ shifts, the substituents of these five complexes were simplified to afford model complexes $II^{LiHMDS'}$, $II^{NaHMDS'}$, **1–12C4'**, **1–15C5'**, and **2-15C5'** (see Computational Details). Our calculations successfully reproduced a slight (overall ca. 9 ppm) but continuous decrease in the observed NMR ^{13}C chemical shifts of the CO_2 ligand from $II^{LiHMDS'}$ to **2–15C5'** (from 183.7 to 174.4 ppm, Table S4), overestimating the overall experimental spread by ~4 ppm. These shifts are substantially larger than the computed (experimental) shift of free CO_2, 124 ppm (126 ppm).[62] Further analyses indicate that the shift decrease correlates with a small but continuous increase of the computed Ni–C distances by 0.02 Å (1.79 to 1.81 Å, Table S5), and a concomitant decrease of the cumulative negative NPA charge on the η^2-CO_2 moiety by ~0.14 a.u. (from −1.06 a.u. to −0.93 a.u., Table S7). The charge on the η^2-CO_2 unit is largely compensated by changes in the (compositionally invariable) Ni-containing molecular fragment (Table S7). Interestingly, the positive ~0.9 a.u. charge of the variable AM fragment of the complexes varies less, by 0.05 a.u. These analyses confirm the assumption that the AM Lewis acid fragment influences both the charge population and the internal charge polarization within the $L^{tBu}Ni(\eta^2$-$CO_2)$ fragment and thereby also modifies the ^{13}C shifts on the carbonite moiety (Figure S137).

Notably, a recent computational study of a rather different set of Ni^0–CO_2 complexes (with pincer ligands)[63] also pointed towards the total net charge on the carbonite fragment as a central determinant of activation, and the charge also correlated with results from energy decomposition analyses. In some of these complexes an Fe^{II}-fragment served as a Lewis acid to withdraw charge from the $LNiCO_2$ moiety, and the effects were rather similar to what we observe for the AM Lewis acid.

C–O bond cleavage

Hence, DFT calculations confirmed that the observed changes of the $\delta^{13}C_{CO_2}$ values indeed correlate with the degree of CO_2 activation, due to a small but notable change in the overall charge population at the CO_2^{2-} ligand. Since "the degree of CO_2 activation" refers to a weakening of one of the C–O bonds, it was expected that the second sphere modifications would also affect the rate of C–O bond cleavage reactions. As previously shown, addition of electrophiles can trigger such a cleavage reaction, causing liberation of CO and transfer of "O^{2-}" to the electrophile (see Scheme 6).[43]

In a report by Agapie et al., a corresponding study was performed on a labile Mo^0–CO_2 adduct.[61] The rate of a proton induced C–O bond cleavage was enhanced by addition of supporting Lewis acids, showing a correlation between the Lewis acidity and the resulting rate constants.

Chemistry–A European Journal

Research Article
doi.org/10.1002/chem.202303112

**Chemistry
Europe**
European Chemical
Societies Publishing

Scheme 6. C—O bond cleavage of the Ni-bound carbonite ligand, triggered by exposure to gaseous CO_2, to form Ni carbonate and carbonyl complexes. The overall reaction proceeds in two steps (black box): 1) C—O bond cleavage under release of CO (E=H^+, Me_3Si^+, CO_2), 2) reductive displacement of CO_2^{2-} by CO.

From our study it was shown that not only the variation of the Lewis acid itself, but also its spatial separation and the introduction of a multifunctional environment affect the Ni^{II}–CO_2^{2-} core. Hence, we were interested whether for a given AM ion these modifications would also impact the kinetics of a C—O bond cleavage. Therefore, reactions between four sodium derivatives (see Figure 12) and external CO_2 as the electrophile were followed by NMR spectroscopy at room temperature to investigate a rate dependency (see SI section 5).

It should be noted that the C—O bond cleavage reaction is in so far not suited for quantitative rate determinations as liberated CO also reacts with unconsumed starting material, to yield a Ni^I carbonyl compound (see Scheme 6, black box). Hence, carbonite complexes are consumed in two competing reactions, preventing calculations of the individual rate constants. Nevertheless, the concentration of CO is limited by a preceding reaction of the complexes with the electrophile, meaning that the overall time needed for full consumption of the starting material is mainly determined by the rate of the initial C—O bond cleavage.

Reaction of **2** with external CO_2 is considered as a benchmark for this study, since **2** represents an unmodified variant of the selected complexes. Full consumption of the starting material was reached 3 h after exposure to CO_2. Monitoring the reaction by ^{13}C NMR spectroscopy revealed that it involves formation of an unknown intermediate, which was again quickly consumed over time. Based on NMR and IR spectroscopic evaluation, nickel carbonate and nickel carbonyl complexes were identified as the mayor products in the final

reaction mixture. C—O bond cleavage was significantly accelerated when **II**^{NaHMDS} was tested instead of **2**. Exposure of the complex to CO_2 resulted in an immediate colour change. An NMR measurement, performed 5 min after CO_2 addition, revealed that the reaction was already completed at this point. However, the reaction involving **II**^{NaHMDS} as the starting complex proceeds in a more complicated fashion, caused by the disilazide function, involving the formation of siloxides (see SI section 5.1 for more detailed explanation). Hence the observed acceleration is not solely caused by a stronger bond activation but also by participation of the co-coordinated amide functions.

While incorporation of additional Na amides caused reduction of the reaction time (Table 1), the opposite was observed when the reaction of **2-THF** was examined, taking about 5 days for complete consumption of the starting material. This effect was even enhanced when **2–15C5** was tested instead, extending the reaction time to about 20 days. Accordingly, within the series of complexes **2**, **2-THF** and **2–15C5** a very significant increase in the reaction time was observed, in line with the decrease in activation as indicated by the $\delta^{13}C_{CO2}$ values.

Since our work so far indicated that the nature of the AM counterion has the most pronounced effect on the CO_2 activation, as indicated by the spectroscopic features, also the derivatives **1-THF** and **3-THF** were subjected to this reactivity study. Upon AM variation an increase in reaction time was observed from Li to K for the THF adducts **1-THF, 2-THF** and **3-THF** indicating that (although no linear regression was found between the spectroscopic parameters as activation measures and the observed reactions times) indeed all second sphere modifications affect the reactivity.

Conclusions

In summary we have shown that increasing the basicity of the amide bases used for formate deprotonation allows isolation of mono metalated nickel carbonite complexes. These complexes turned out to be ideal platforms for modifications of the second coordination sphere around the Ni^{II}–CO_2^{2-} core. Based on the resulting series of complexes an in-depth study on the effect of those modifications on CO_2 activation was performed. Apart from variation of the Lewis acidic counterion also the spatial separation between the cooperating sites and the construction of multifunctional sites has been examined for the first time. The combination of these "tools" was found to enable a
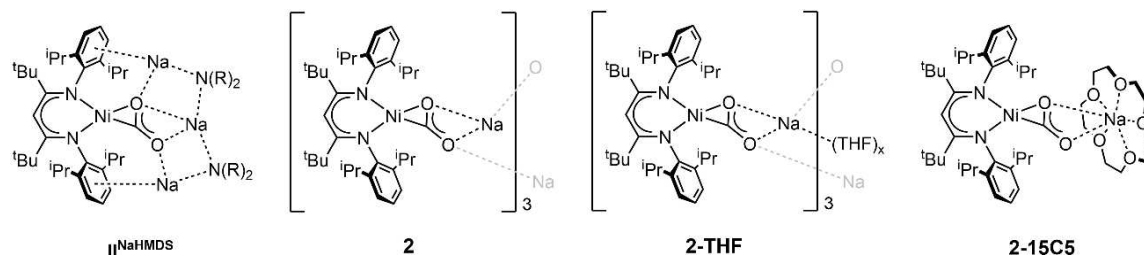

Figure 12. Selected complexes for the C—O bond cleavage study.

Chemistry–A European Journal

Research Article
doi.org/10.1002/chem.202303112

Chemistry Europe
European Chemical
Societies Publishing

Table 1. Reaction time of the C–O bond cleavage study.

	$\delta^{13}C_{CO2}$ [ppm]	Reaction time
II^{NaHMDS}	173.2 (C_6D_6)	< 5 min
2	175.9 (C_6D_6)	3 h
1-THF	170.7 (THF-d_8)	60 h
2-THF	170.5 (THF-d_8)	5 d
3-THF	169.3 (THF-d_8)	9 d
2-15C5	168.6 (C_6D_6)	~20 d

modular fine tuning for the degree of CO_2 activation, which is reflected not only by the spectroscopic and structural features of the complexes but also in the reactivity: the extent of activation determines the rates of the C–O bond cleavage in contact with electrophiles.

A relativistic DFT study of a subset of complexes, with focus on the $^{13}C(CO_2)$ NMR shifts, shows that the coordinating AM Lewis acid fragment withdraws only a small amount of charge from the carbonite moiety, but it also affects the internal charge equilibration between the $L^{tBu}Ni$ and carbonite moieties. This is accompanied also by structural changes, in particular in the Ni–C bond length to the carbonite ligand.

The results of this study therefore provide useful information for the design of catalysts for CO_2 reduction showing how secondary interaction might affect the performance. As the nature of the counterion was found to have a significant influence future research will focus on the extension of the cooperative metals from AM ions to earth alkaline and even transition metal ions.

Supporting Information

The authors have cited additional references within the Supporting Information.[64–83] General considerations, synthetic procedures and characterisation, supporting data to assess the degree of CO_2 activation, DOSY measurements, C–O splitting reaction details, computational details, crystallographic data, cartesian coordinates of the DFT-optimized models, animated normal modes.

Conflict of Interests

The authors declare no conflict of interest.

Data Availability Statement

The data that support the findings of this study are available in the supplementary material of this article.

[1] G. A. Olah, *Angew. Chem. Int. Ed.* **2005**, *44*, 2636–2639.
[2] G. Centi, S. Perathoner, *Catal. Today* **2009**, *148*, 191–205.
[3] M. Aresta, A. Dibenedetto, A. Angelini, *J. CO2 Util.* **2013**, *3–4*, 65–73.
[4] J. Artz, T. E. Müller, K. Thenert, J. Kleinekorte, R. Meys, A. Sternberg, A. Bardow, W. Leitner, *Chem. Rev.* **2018**, *118*, 434–504.
[5] E. A. Quadrelli, G. Centi, J.-L. Duplan, S. Perathoner, *ChemSusChem* **2011**, *4*, 1194–1215.
[6] R. Schlögl, *Angew. Chem. Int. Ed.* **2022**, *61*, e202007397.
[7] X. Yin, J. R. Moss, *Coord. Chem. Rev.* **1999**, *181*, 27–59.
[8] J. Ma, N. Sun, X. Zhang, N. Zhao, F. Xiao, W. Wei, Y. Sun, *Catal. Today* **2009**, *148*, 221–231.
[9] M. Rakowski Dubois, D. L. Dubois, *Acc. Chem. Res.* **2009**, *42*, 1974–1982.
[10] H.-Q. Liang, T. Beweries, R. Francke, M. Beller, *Angew. Chem. Int. Ed.* **2022**, *61*, e202200723.
[11] S.-T. Bai, G. De Smet, Y. Liao, R. Sun, C. Zhou, M. Beller, B. U. W. Maes, B. F. Sels, *Chem. Soc. Rev.* **2021**, *50*, 4259–4298.
[12] H. H. Cramer, S. Das, M. D. Wodrich, C. Corminboeuf, C. Werlé, W. Leitner, *Chem. Sci.* **2023**, *14*, 2799–2807.
[13] N. W. Kinzel, C. Werlé, W. Leitner, *Angew. Chem. Int. Ed.* **2021**, *60*, 11628–11686.
[14] M. Marx, H. Frauendorf, A. Spannenberg, H. Neumann, M. Beller, *JACS Au* **2022**, *2*, 731–744.
[15] J. Shi, Y. Jiang, Z. Jiang, X. Wang, X. Wang, S. Zhang, P. Han, C. Yang, *Chem. Soc. Rev.* **2015**, *44*, 5981–6000.
[16] A. M. Appel, J. E. Bercaw, A. B. Bocarsly, H. Dobbek, D. L. DuBois, M. Dupuis, J. G. Ferry, E. Fujita, R. Hille, P. J. A. Kenis, C. A. Kerfeld, R. H. Morris, C. H. F. Peden, A. R. Portis, S. W. Ragsdale, T. B. Rauchfuss, J. N. H. Reek, L. C. Seefeldt, R. K. Thauer, G. L. Waldrop, *Chem. Rev.* **2013**, *113*, 6621–6658.
[17] A. Paparo, J. Okuda, *J. Organomet. Chem.* **2018**, *869*, 270–274.
[18] J.-H. Jeoung, H. Dobbek, *Science* **2007**, *318*, 1461–1464.
[19] J. Fesseler, J.-H. Jeoung, H. Dobbek, *Angew. Chem. Int. Ed.* **2015**, *54*, 8560–8564.
[20] W. Leitner, *Coord. Chem. Rev.* **1996**, *153*, 257–284.
[21] D. H. Gibson, *Coord. Chem. Rev.* **1999**, *185–186*, 335–355.
[22] M. R. Crimmin, R. Y. Kong, N. Phillips, in *Comprehensive Coordination Chemistry III* (Eds.: E. C. Constable, G. Parkin, L. Que Jr), Elsevier, Oxford **2021**, p. 311–362.
[23] M. Perez-Jimenez, H. Corona, F. de la Cruz-Martínez, J. Campos, *Chem. Eur. J.* **2023**, *29*, e202301428.
[24] F. Schneck, J. Ahrens, M. Finger, A. C. Stückl, C. Würtele, D. Schwarzer, S. Schneider, *Nat. Commun.* **2018**, *9*, 1161.
[25] C. Yoo, Y. E. Kim, Y. Lee, *Acc. Chem. Res.* **2018**, *51*, 1144–1152.
[26] B. M. Puerta Lombardi, C. Gendy, B. S. Gelfand, G. M. Bernard, R. E. Wasylishen, H. M. Tuononen, R. Roesler, *Angew. Chem. Int. Ed.* **2021**, *60*, 7077–7081.
[27] T.-W. Chiou, Y.-M. Tseng, T.-T. Lu, T.-C. Weng, D. Sokaras, W.-C. Ho, T.-S. Kuo, L.-Y. Jang, J.-F. Lee, W.-F. Liaw, *Chem. Sci.* **2016**, *7*, 3640–3644.
[28] A. W. Nichols, C. W. Machan, *Front. Chem.* **2019**, *7*.
[29] S. Bagherzadeh, N. P. Mankad, *J. Am. Chem. Soc.* **2015**, *137*, 10898–10901.
[30] E. A. Bielinski, P. O. Lagaditis, Y. Zhang, B. Q. Mercado, C. Würtele, W. H. Bernskoetter, N. Hazari, S. Schneider, *J. Am. Chem. Soc.* **2014**, *136*, 10234–10237.
[31] O. Cooper, C. Camp, J. Pécaut, C. E. Kefalidis, L. Maron, S. Gambarelli, M. Mazzanti, *J. Am. Chem. Soc.* **2014**, *136*, 6716–6723.
[32] A. Paparo, J. S. Silvia, T. P. Spaniol, J. Okuda, C. C. Cummins, *Chem. Eur. J.* **2018**, *24*, 17072–17079.
[33] J. M. Barlow, J. Y. Yang, *ACS Cent. Sci.* **2019**, *5*, 580–588.
[34] H. Corona, M. Pérez-Jiménez, F. de la Cruz-Martínez, I. Fernández, J. Campos, *Angew. Chem. Int. Ed.* **2022**, *61*, e202207581.
[35] A. R. Sadique, W. W. Brennessel, P. L. Holland, *Inorg. Chem.* **2008**, *47*, 784–786.

Chemistry–A European Journal

Research Article
doi.org/10.1002/chem.202303112

Chemistry Europe
European Chemical
Societies Publishing

[36] B. Horn, C. Limberg, C. Herwig, B. Braun, *Chem. Commun.* **2013**, *49*, 10923–10925.

[37] L. Roy, M. H. Al-Afyouni, D. E. DeRosha, B. Mondal, I. M. DiMucci, K. M. Lancaster, J. Shearer, E. Bill, W. W. Brennessel, F. Neese, S. Ye, P. L. Holland, *Chem. Sci.* **2019**, *10*, 918–929.

[38] P. M. Jurd, H. L. Li, M. Bhadbhade, L. D. Field, *Organometallics* **2020**, *39*, 2011–2018.

[39] P. Zimmermann, A. F. R. Kilpatrick, D. Ar, S. Demeshko, B. Cula, C. Limberg, *Chem. Commun.* **2021**, *57*, 875–878.

[40] A.-C. Schmidt, A. V. Nizovtsev, A. Scheurer, F. W. Heinemann, K. Meyer, *Chem. Commun.* **2012**, *48*, 8634–8636.

[41] P. Zimmermann, S. Hoof, B. Braun-Cula, C. Herwig, C. Limberg, *Angew. Chem. Int. Ed.* **2018**, *57*, 7230–7233.

[42] N. J. Hartmann, G. Wu, T. W. Hayton, *Chem. Sci.* **2018**, *9*, 6580–6588.

[43] P. Zimmermann, D. Ar, M. Rossler, P. Holze, B. Cula, C. Herwig, C. Limberg, *Angew. Chem. Int. Ed. Engl.* **2021**, *60*, 2312–2321.

[44] V. H. Gessner, C. Däschlein, C. Strohmann, *Chem. Eur. J.* **2009**, *15*, 3320–3334.

[45] A. Harrison-Marchand, F. Mongin, *Chem. Rev.* **2013**, *113*, 7470–7562.

[46] H. J. Reich, *Chem. Rev.* **2013**, *113*, 7130–7178.

[47] J. W. Steed, *Coord. Chem. Rev.* **2001**, *215*, 171–221.

[48] C. Yoo, Y. Lee, *Chem. Sci.* **2017**, *8*, 600–605.

[49] D. W. Stephan, *J. Am. Chem. Soc.* **2015**, *137*, 10018–10032.

[50] D. W. Stephan, G. Erker, *Chem. Sci.* **2014**, *5*, 2625–2641.

[51] S. P. S. K. Mandal, *Chem. Sci.* **2020**, *11*, 10571–10593.

[52] F.-G. Fontaine, M.-A. Courtemanche, M.-A. Légaré, É. Rochette, *Coord. Chem. Rev.* **2017**, *334*, 124–135.

[53] M. Sakamoto, I. Shimizu, A. Yamamoto, *Organometallics* **1994**, *13*, 407–409.

[54] M. Aresta, C. F. Nobile, V. G. Albano, E. Forni, M. Manassero, *J. Chem. Soc. Chem. Commun.* **1975**, 636–637.

[55] I. Castro-Rodriguez, H. Nakai, L. N. Zakharov, A. L. Rheingold, K. Meyer, *Science* **2004**, *305*, 1757–1759.

[56] Y. E. Kim, J. Kim, Y. Lee, *Chem. Commun.* **2014**, *50*, 11458–11461.

[57] M. Devillard, R. Declercq, E. Nicolas, A. W. Ehlers, J. Backs, N. Saffon-Merceron, G. Bouhadir, J. C. Slootweg, W. Uhl, D. Bourissou, *J. Am. Chem. Soc.* **2016**, *138*, 4917–4926.

[58] K. Lee, J. Choi, P. M. Graham, Y. Lee, *Bull. Korean Chem. Soc.* **2022**, *43*, 222–226.

[59] S. Sakaki, A. Dedieu, *Inorg. Chem.* **1987**, *26*, 3278–3284.

[60] S. Sinhababu, M. R. Radzhabov, J. Telser, N. P. Mankad, *J. Am. Chem. Soc.* **2022**, *144*, 3210–3221.

[61] J. A. Buss, D. G. VanderVelde, T. Agapie, *J. Am. Chem. Soc.* **2018**, *140*, 10121–10125.

[62] W. Makulski, *Phys. Chem. Chem. Phys.* **2022**, *24*, 8950–8961.

[63] J. Park, M. Cho, Y. M. Rhee, Y. Jung, *ACS Omega* **2021**, *6*, 7646–7654.

[64] J. T. L. Lochmann, *J. Organomet. Chem.* **1979**, *179*, 123–132.

[65] M. J. Frisch, G. W. Trucks, H. B. Chlegel, G. E. Scuseria, M. A. Robb, J. R. Cheeseman, G. Scalmani, V. Barone, G. A. Petersson, H. Nakatsuji, X. Li, M. Caricato, A. V. Marenich, J. Bloino, B. G. Janesko, R. Gomperts, B. Mennucci, H. P. Hratchian, J. V. Ortiz, A. F. Ismaylov, J. L. Sonnenberg, D. Williams-Young, F. Ding, F. Lipparini, F. Egidi, J. Goings, B. Peng, A. Petrone, T. Henderson, D. Ranasinghe, V. G. Zakrzewski, J. Gao, N. Rega, G. Zheng, W. Liang, M. Hada, M. Ehara, K. Toyota, R. Fukuda, J. Hasegawa, M. Ishida, T. Nakajima, Y. Honda, O. Kitao, H. Nakai, T. Vreven, K. Throssell, J. A. Montgomery, J. E. Peralta, F. Ogliaro, M. Bearpark, J. J. Heyd, E. Brothers, K. N. Kudin, V. N. Staroverov, T. Keith, R. Kobayashi, J. Normand, K. Raghavachari, A. Rendell, J. C. Burant, S. S. Iyengar, J. Tomasi, M. Cossi, J. M. Millam, M. Klene, C. Adamo, R. Cammi, J. W. Ochterski, R. L. Martin, K. Morokuma, O. Farkas, J. B. Foresman, D. J. Fox, *Gaussian 09, revision D.01*, Gaussian, Inc., Wallingford CT **2016**.

[66] V. N. Staroverov, G. E. Scuseria, J. Tao, J. P. Perdew, *J. Chem. Phys.* **2003**, *119*, 12129–12137.

[67] V. N. Staroverov, G. E. Scuseria, J. Tao, J. P. Perdew, *J. Chem. Phys.* **2004**, *121*, 11507.

[68] F. Weigend, R. Ahlrichs, *Phys. Chem. Chem. Phys.* **2005**, *7*, 3297–3305.

[69] S. Grimme, J. Antony, S. Ehrlich, H. Krieg, *J. Chem. Phys.* **2010**, *132*, 154104.

[70] S. Grimme, S. Ehrlich, L. Goerigk, *J. Comput. Chem.* **2011**, *32*, 1456–1465.

[71] J. Tomasi, B. Mennucci, R. Cammi, *Chem. Rev.* **2005**, *105*, 2999–3084.

[72] V. Pelmenschikov, Y. Guo, H. Wang, S. P. Cramer, D. A. Case, *Faraday Discuss.* **2011**, *148*, 409–420.

[73] NBO 6.0.18a, E. D. Glendening, J. K. Badenhoop, A. E. Reed, J. E. Carpenter, J. A. Bohmann, C. M. Morales, P. Karafiloglou, C. R. Landis, F. Weinhold, Theoretical Chemistry Institute, University of Wisconsin, Madison, WI **2018**.

[74] A. E. Reed, L. A. Curtiss, F. Weinhold, *Chem. Rev.* **1988**, *88*, 899–926.

[75] M. Repisky, S. Komorovsky, V. G. Malkin, O. L. Malkina, M. Kaupp, K. Ruud, R. Bast, R. Di Remigio, U. Ekstrom, M. Kadek, S. Knecht, L. Konecny, ReSpect 5.1.0 Relativistic Spectroscopy DFT program **2019**, http://www.respectprogram.org.

[76] T. W. Keal, D. J. Tozer, *J. Chem. Phys.* **2003**, *119*, 3015–3024.

[77] W. Kutzelnigg, U. Fleischer, M. Schindler, "The IGLO-Method: Ab-initio calculation and interpretation of NMR chemical shifts and magnetic susceptibilities" in *Deuterium and Shift Calculation*, P. Diehl, E. Fluck, H. Günther, R. Kosfeld, J. Seelig, Eds. (Springer, Berlin **1991**); vol. 23 of *NMR Basic Principles and Progress*, pp. 165–262.

[78] K. G. Dyall, *Theor. Chem. Acc.* **2006**, *115*, 441–447.

[79] G. M. Sheldrick, SADABS **1996**, University of Göttingen, Germany.

[80] G. M. Sheldrick, *Acta Crystallogr. Sect. A* **2015**, *71*, 3.

[81] G. M. Sheldrick, *Acta Crystallogr. Sect. C* **2015**, *71*, 3.

[82] C. B. Hübschle, G. M. Sheldrick, B. Dittrich, *J. Appl. Crystallogr.* **2011**, *44*, 1281–1284.

[83] A. L. Spek, *Acta Crystallogr. Sect. D* **2009**, *65*, 148.